Simulating tip effects in vertical-axis wind turbines with the actuator line method

Simulating tip effects in vertical-axis wind turbines with the actuator line method

PF Melani[1], F Balduzzi[1], A Bianchini[1]

[1] Department of Industrial Engineering, Università degli Studi di Firenze, Via di Santa Marta 3, 50139, Firenze, Italy.

Corresponding author: alessandro.bianchini@unifi.it

Abstract. Simulation of the complex, unsteady aerodynamics characterizing Darrieus rotors requires computational tools with a fidelity higher than the ubiquitous Blade Element Momentum (BEM) theory. Among them, the Actuator Line Method (ALM) stands out in terms of accuracy and computational cost. This approach, however, still fails to resolve the vortex-like structures shed at the blade ends, overestimating turbine performance at the higher rotational speeds. Moving from this background, in this study a comprehensive investigation on the ALM's capability to simulate tip effects and their impact on rotor performance is carried out. To this end, the ALM tool developed by the authors in the ANSYS® FLUENT® environment (v. 20.2) and specifically tailored to the simulation of vertical-axis machines was employed. Both a steady finite wing and a fictitious one-blade Darrieus H-rotor, for which high-fidelity blade-resolved CFD data are available as benchmark, were considered as test cases. ALM simulations were first performed without any correction for different cell sizes and force projection radii, so that the limits of the original approach could be assessed. Then, two different sub-models were applied: the classical semi-empirical Glauert correction and a new methodology based on the Lifting Line Theory (LLT), which was recently proposed by Dağ and Sørensen (DS). The latter was here adapted to vertical-axis machines. Eventually, the blade spanwise load profiles coming from the three approaches were assessed and compared, proving the superior performance of the DS model.

Keywords: Darrieus, VAWT, ALM, CFD, Tip effects

1. Introduction and objectives of the study

Simulation of the complex aerodynamics of Darrieus rotors, characterized by a continuous oscillation of the blade angle of attack, often exceeding the static stall limit [1], requires computational tools with a fidelity higher than the ubiquitous Blade Element Momentum (BEM) theory. Among them, the Actuator Line Method (ALM) [2], which combines a lumped-parameter representation of the rotor blades with the resolution of the local flow field via Computational Fluid Dynamics (CFD), stands out in terms of ratio between accuracy and computational cost. This approach, however, still falls behind other medium-fidelity methodologies such as the Lifting Line Theory (LLT) [3] when it comes to resolve the vortex-like structures shed at the blade end (i.e., tip vortexes) and their effect on the blade

spanwise load profile. This accuracy gap is particularly evident when simulating higher Tip-Speed Ratios (TSRs), where the ALM tends to largely overestimate the rotor power production [5].

Different approaches have proposed over the years to overcome this issue. In their trailblazing work, Shives and Crawford [4] investigated the effect of different kernel widths β and grid resolutions on the predicted load distribution over a fixed-wing case, concluding that a chord-based kernel width β≈0.25c is the necessary condition for the proper simulation of tip vortexes with the ALM. As in that work the local inflow velocity is sampled at the center of the actuator line, a constraint on the ALM element size $h_{ALM} < 0.25\beta$ was also added to avoid distortion of the computed angle of attack. These results were later confirmed for the simulation of horizontal-axis wind turbines (HAWTs) by Martínez-Tossas [5] and Jha et al. [6], who also proposed to improve the predicted circulation distribution along the blade by reducing the kernel width towards the tip with an elliptical law. The concept was pushed further by Churchfield et al. [7], by replacing the standard isotropic Gaussian smearing function with an arbitrary one, varying in the airfoil chord-wise and thickness-wise directions to better resemble the actual blade shape. Although effective, both methodologies require case-specific tuning and finer grids than the baseline ALM. In order to overcome the stricter mesh requirements associated to the direct ALM simulation of tip vortexes and minimize the dependence on the kernel width value, researchers at the National Renewable Energy Laboratory (NREL) [8] and Danmarks Tekniske Universitet (DTU) [9,10] recently introduced a novel hybrid tip loss model. The latter makes use of LLT to compute the contribution to the downwash induced by tip vortexes, which is lost in the ALM due to the characteristic smearing of the blade forces in the computational domain, yielding accurate results without increasing the approach set-up and computational effort.

Moving from this background, the current paper presents the prediction capability of the ALM to simulate tip effects and their impact on VAWT performance. In the authors' knowledge, this is the first study to be carried out on the subject. To this end, the ALM tool developed by the authors and tailored to the simulation of vertical-axis machines [11] was employed for both a steady finite wing and a fictitious one-blade Darrieus H-rotor, for which blade-resolved CFD data are available as benchmark [12]. ALM simulations were first performed without any correction (*baseline*) for different cell sizes and force projection radii, so that the limits of the original approach could be assessed. Then, two different sub-models were applied: the classical semi-empirical Glauert correction for tip losses [13] and a new methodology recently proposed by Dağ and Sørensen (DS) for HAWTs [9] and here adapted to VAWTs. Eventually, the blade spanwise load profiles coming from the three methods were compared.

2. Methodology

2.1. Actuator Line Method (ALM)

In the present work, the ALM module developed by the authors in the ANSYS® FLUENT® solver, version 20.2, and specifically tailored for the simulation of vertical-axis machines [11], was adopted. More in detail, this code features a novel *LineAverage* [14] method for sampling the angle of attack, in which the undisturbed velocity $\boldsymbol{V}$ is computed as the integral average of the flow velocity field along a circular sampling line, centered in the airfoil quarter-chord and with a radius r=1c. The computed aerodynamic forces on the other hand are spread into the domain via the standard isotropic two-dimensional Gaussian kernel. The corresponding width β is related to an airfoil characteristic dimension, i.e. chord c, as in [4]. Various sub-models are also available in the code to account for VAWT specific effects, such as the contribution of pitching moment to torque, the effect of the Blade-Spoke Connection (BSC) position and dynamic stall.

2.2. Finite wing simulations

For fixed-wing tests, a fictitious NACA0018 blade was selected, with a chord c=0.382 m and three different Aspect Ratios AR=c/H ∈ [10 14 20]. The latter was simulated for a chord-based Reynolds number of $Re_c=550x10^3$ and angle of attack α=6°, via a blade-resolved and an ALM approach. Numerical set-up is the same for both cases and is based on a consolidated numerical approach

developed by some of the authors for airfoil simulation [15]. More in detail, steady Reynolds-Averaged Navier-Stokes (RANS) CFD simulations were carried out with the ANSYS® Fluent® (v. 20.2) solver, making use of the k-ω SST turbulence model, the coupled algorithm for pressure-velocity coupling, and the 2nd order upwind scheme for both RANS and turbulence equations.

The computational domain has an open field configuration, with an overall extent of L = 60c and a width of W = 40c and a height of H_D= 3H to avoid blockage effects and allow the proper development of the wake (see Figure 1). In order to reduce the overall number of elements, the spanwise symmetry of the problem was exploited, simulating only half of the domain. At its boundaries, the standard far field boundary conditions for external flows are applied: uniform velocity at the inlet boundary, ambient pressure at the outlet one, symmetry on the other surfaces. For blade-resolved simulations, the smooth no-slip wall condition was added for the blade surface.

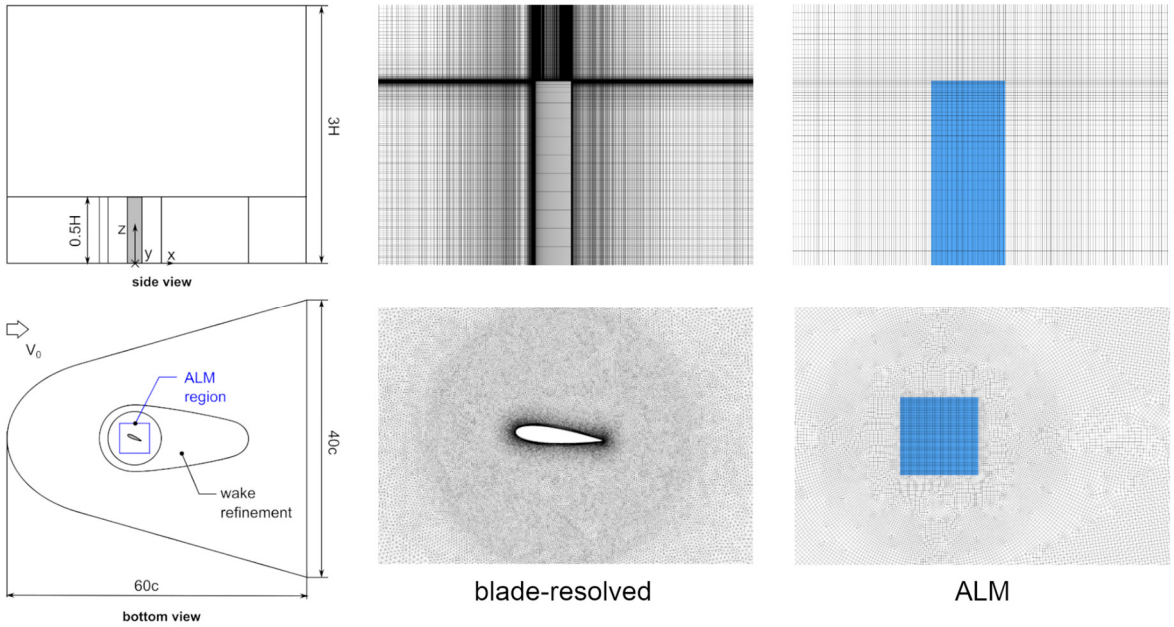

Figure 1. Overview of the mesh for the blade-resolved and ALM approaches

The discretization of the computational domain followed two different approaches, based on the selected method. For blade-resolved simulations, an unstructured, triangular mesh was built on the bottom plane, according to the experience of the authors on similar test cases [15], with local refinements in proximity of the airfoil and its wake. In order to guarantee the correct resolution of the blade boundary layer, an O–grid of 720 quadrilateral elements was used around its surface, with a dimensionless wall distance (y^+) lower than ~ 1 and a total number of layers of 40. The bottom mesh was then extruded in the spanwise direction along the blade, employing 150, 190 or 250 layers depending on the aspect ratio, and distributing them according to an exponential bias to optimize the grid density at the tip [12].

Overall, the same strategy was followed for the ALM, replacing triangular elements with quadrilateral ones on the bottom plane. A uniform structured grid was used instead for the blade region (see Figure 1), as required by the ALM approach, with a minimum resolution of $h_{ALM} = 0.4\beta$ for stability reasons. The elements in the wake and external domain were scaled accordingly. For further details regarding the adopted meshing strategy, please refer to [11]. In order to understand the influence of the ALM grid on the predicted loads and tip vortex structures, a dedicated sensitivity analysis was performed, whose results are shown in Section 3.2. More in detail, as reported in Table 1, eight different meshes, distinguished in terms of kernel width β and spanwise resolution (both in terms of number of elements and bias factor), were tested.

Table 1. ALM meshes

Dimension	B01	B02	B03	B01b	B03b	B11	B12	B13	B11b	B13b
β/c [-]	0.2	0.2	0.2	0.2	0.2	0.1	0.1	0.1	0.1	0.1
# spanwise elements	30	60	80	30	80	30	60	80	30	80
spanwise bias factor	1	1	1	1.08	1.08	1	1	1	1.08	1.08
# cells [k]	2085	3397	3898	1949	4456	4763	7749	8891	4347	9937

2.3. Rotor simulations

For rotor simulations, it was considered as test case the fictitious one-blade variant of a prototype three-blade machine, extensively tested in the experimental facility of the Politecnico di Milano by Dossena et al. [16]. The rotor is characterized by a diameter D=0.515m and height H=1.457m, while the blade is a NACA0021 profile with a chord c=0.086. The resulting Aspect Ratio is AR≈17. The selection of this particular turbine is justified by the low solidity and the availability of detailed wake velocity and blade spanwise loading data for a high-load operating point (TSR=3.3, V_0=9m/s), coming from the high-fidelity, three-dimensional blade-resolved CFD simulations of Balduzzi et al. [12]. The corresponding polar data was obtained with the viscous panel method XFoil [17] in the attached flow region and then extended to ±180° via the Viterna-Corrigan formulation. In the process, flow curvature effects were accounted for via proper conformal mapping of the geometric airfoil [18].

All three-dimensional simulations were carried out with an unsteady Reynolds-Averaged Navier-Stokes (URANS) approach via the commercial solver ANSYS® FLUENT®, in the 20.2 release, coupled with the ALM methodology described in Section 2.1, making use of the k-ω SST turbulence model. The angular timestep was set to Δθ=1°. In the same fashion of fixed-wing simulations (see Section 2.2), an open field approach was used for the setting of the computational domain and boundary conditions, while the mesh was divided in a structured ALM region and an unstructured external one. The element size corresponding to each region was proportionally scaled to the kernel width β, which for this case was selected based on fixed-wing simulations (see Section 3.2). For further details about numerical set-up and meshing strategy, please refer to [11].

2.4. End effects corrections

The tip loss corrections selected for this work represents the two extremes of the wide spectrum of methods available in the literature. The former is the analytical formulation by Glauert, employed in the majority of aerodynamic codes for its simplicity and robustness, but now inadequate for the simulation of modern rotors. The latter is a novel hybrid methodology developed by Dağ and Sørensen, which employs NLLT to provide a more general and physically sound description of end effects. On top of that, this correction was specifically designed for the ALM.

2.4.1. Glauert correction. The Glauert correction [13] belongs to a family of analytical approaches originally developed for HAWTs and that is currently used to account for tip losses in the majority of BEM codes, although with various semi-empirical modifications (e.g. the Shen correlation [19]). This approach is based on the definition of a factor F ∈ [0 1], which is used to correct the rotor forces (or in the case of the BEM, the induction coefficient). The computation of this factor is based on a potential model of the turbine wake, under the assumption of no expansion and/or distortion. Therefore, it suited only for lightly-loaded rotors. In the current work, the original formula was adapted to the use with vertical-axis machines:

$$F(z) = \frac{2}{\pi} \cdot \arccos\left[exp\left(-\frac{1}{2}\frac{N_b(H-z)}{z \cdot sin(\alpha)}\right)\right] \quad (1)$$

where z is the blade spanwise coordinate, N_b the number of blades and H the rotor height. In the present ALM tool, the correction is applied to the computed blade forces. Although, from the authors point of

view, this methodology has a degree of approximation that is not acceptable for the simulation of VAWTs, it represents a good example of the current state-of-the-art for tip losses modelling. Therefore, in the current work it was selected as a reference for the comparison with the more advanced Dağ-Sørensen correction.

2.4.2. Dağ-Sørensen (DS) correction. The Dağ-Sørensen correction is based on the observation that, when using an isotropic Gaussian smearing function, the insertion of ALM forces has the same effect on the local flow field of a Lamb-Oseen vortex with a viscous radius equal to the force projection width β [9]. The same vorticity pattern is propagated to the vortex sheet developing in the airfoil wake, which is responsible for the downwash effect commonly associated to tip vortexes. As shown in Figure 2 nonetheless, the presence of the viscous core results in an underestimation of the downwash magnitude with respect to the ideal inviscid case represented by the LLT solution. For this reason, the ALM tends to overestimate the blade loading approaching the blade tip.

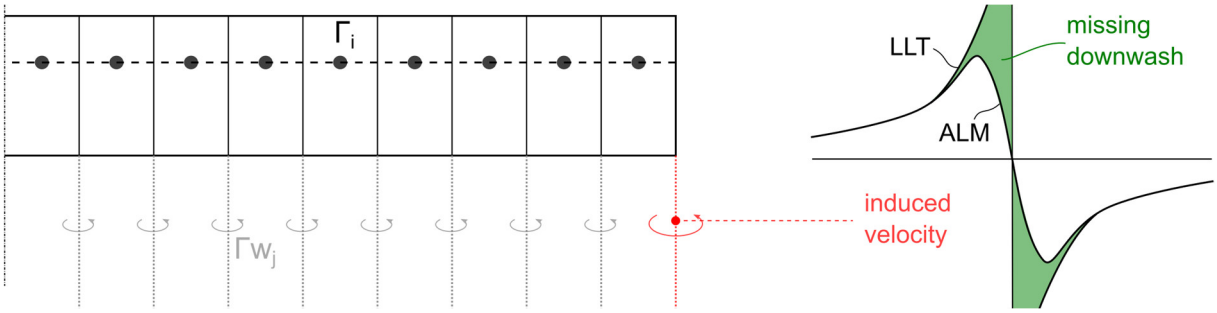

Figure 2. Schematic representation of the Dağ-Sørensen correction

This issue can be overcome by computing the induced velocity distribution associated to each trailing vortex element from the analytical formulations of the Lamb-Oseen and inviscid vortexes and scaling it with the local circulation Γw_j. The latter is obtained as the circulation difference Γ_{i+1}- Γ_i between two adjacent ALM elements. The downwash for each i-th cell $w_{corr,i}$ is then obtained by summing the contributions along the whole blade span, as in Eq. 2:

$$w_{corr,i} = \sum_{j=1}^{N+1} \frac{\Gamma w_j}{4\pi d_{ij}} \cdot \exp\left(-\frac{d_{ij}^2}{\beta^2}\right) \tag{2}$$

where d_{ij} is the distance between the i-th ALM and the j-th vortex element. The angle of attack for each ALM elements can be eventually calculated as:

$$\alpha_i = \alpha_{g,i} - \alpha_{w,i} = \alpha_{g,i} - \frac{w_{corr,i}}{V_{rel,i}} \tag{3}$$

where $\alpha_{g,i}$ is the angle of attack sampled from the ALM simulation, while $\alpha_{w,i}$ is the downwash angle, obtained from the ratio between $w_{corr,i}$ and the ALM element relative velocity $V_{rel,i}$. This is valid under the assumption that the computed incidence remains relatively small ($\tan \alpha_w \approx \alpha_w$).
Due to the strongly non-linear nature of the problem, the latter needs to be resolved in an iterative way. For the purpose, in this work the algorithm developed by Anderson [20] for the Nonlinear Lifting Line Theory (NLLT) was employed. More in detail:

1. an initial circulation distribution $\Gamma_0(z)$ is computed from the sampled angle of attack one
2. the angle of attack distribution is evaluated based on Eqs. 2-3
3. the circulation along the blade span is updated via the Kutta-Joukowsky condition, i.e. $\Gamma_i = 0.5 \cdot C_{L,i}(\alpha_i) \cdot cV_{rel,i}$. In this work in particular, for stability reasons, the relationship between the lift coefficient $C_{L,i}$ and the angle of attack is assumed to be linear, $C_{L,i} = m \cdot \alpha_i$

4. under-relaxation is applied, $\Gamma_{i,new} = \Gamma_i + D \cdot (\Gamma_{i,new} - \Gamma_i)$, with D = 0.05 [20]

Steps 2-4 are repeated until the circulation error $\Gamma_{i,new} - \Gamma$ is reduced below a certain tolerance, here taken as 10^{-3}. It must be noted that the procedure described so far, in contrast with the original work of Dağ and Sørensen [9], does not account for the contribution of the vorticity shed in the wake. For Darrieus machines in fact, the vortex lines shed by the blades tend to self-intersect as the wake develops downstream, making the evaluation of the corresponding induced velocity extremely challenging.

3. Results

3.1. Tip vortex tracking metrics. In order to quantify the effect of the various modelling strategies on the predicted tip vortex structure, different vortex tracking metrics were selected from the literature. More in detail, the following quantities of interest, as illustrated in Figure 3, were defined:

- *vortex center C*: the vortex center defines the axis of rotation of the vortical structure and it is used to track the position of the vortex filament over time. In the present work, this quantity is extracted from the resolved flow field as the minimum of the λ_2 scalar field [21]. This strategy allows in fact to filter out the contribution of viscous stresses and irrotational straining.
- *vortex core radius r_C*: the vortex core radius defines the extension of the rotational region, highlighted in Figure 3, in which the fluid particles are characterized by a rigid body motion. This corresponds to an elevated concentration of vorticity. In the present work, this value is exploited to quantify the vortex aging, i.e. viscous decay, in the wake and is computed as the distance between the vortex center C and the point of maximum induced velocity V_{ind} sampled on a plane normal to the vortex line [22], as in Figure 3.
- *vortex circulation Γ_V:* circulation is a measure of the vortex intensity and is used together with r_C to measure its aging in the wake. In this work, it was computed as the integral of the in-plane vorticity ω_x over a plane normal to the vortex line. In order to avoid the inclusion of spurious contributions, the integration domain was limited to a radius of 2c from the vortex center.

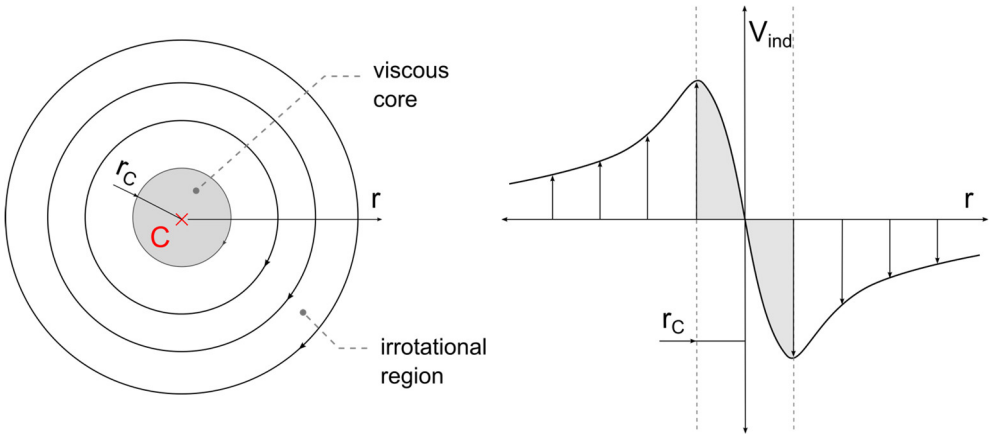

Figure 3. Schematic representation of the tip vortex structure

3.2. Finite-wing simulations

In order to understand the effect of mesh resolution and kernel width β/c on the blade loads and tip vortex structure predicted by the *baseline* ALM formulation, i.e., without corrections, eight different grids (see Table 1) were tested on the fixed-wing test case, for AR=10 and α=6°. Figure 4 reports the comparison in terms of spanwise lift coefficient and downwash velocity V_y, sampled at 1c distance from the airfoil aerodynamic center, between ALM and blade-resolved CFD. At first glance, it can be observed how the coarser meshes (BX1) are not adequate to resolve the blade 3-D field.

This trend is confirmed by Figure 5, for the core radius r_C and circulation Γ. Increasing the resolution towards the blade tip, the ALM downwash profile converges towards the CFD one, both in terms of

constant value along the blade w_0 and peak value, with a small influence of β/c. The best agreement is obtained with the biased grids (BXXb), even though the downwash gradient in the last 10% of the blade is still largely underestimated. The effect of the spanwise discretization on the tip vortex structure in the wake is on the other hand quite limited, as shown in Figure 5. Beyond a certain threshold in fact, given by the BX1 grids, all meshes approximately converge towards the same value of vortex intensity Γ, matching the one predicted by blade-resolved simulations.

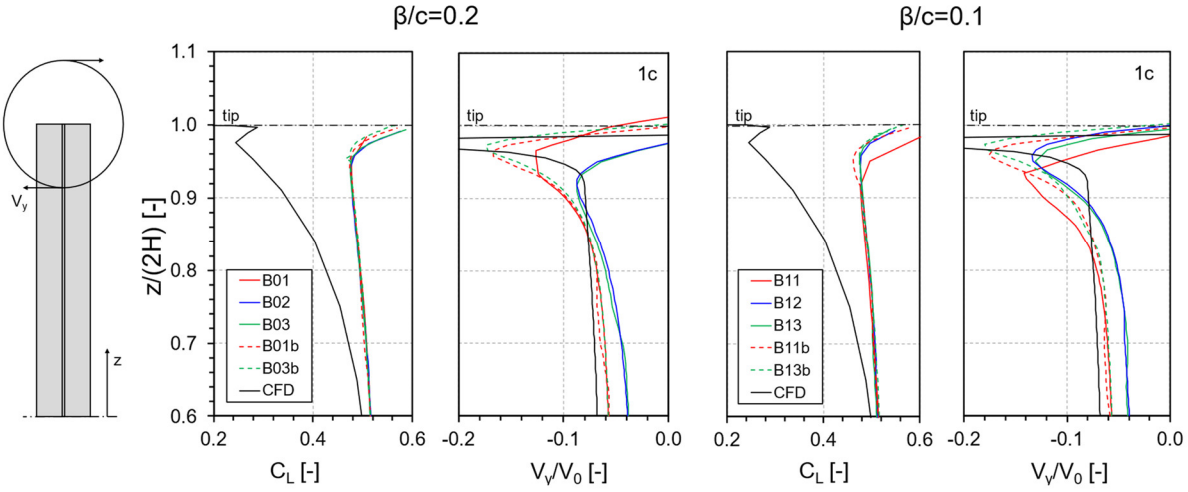

Figure 4. Comparison between baseline ALM and CFD in terms of blade loading and downwash

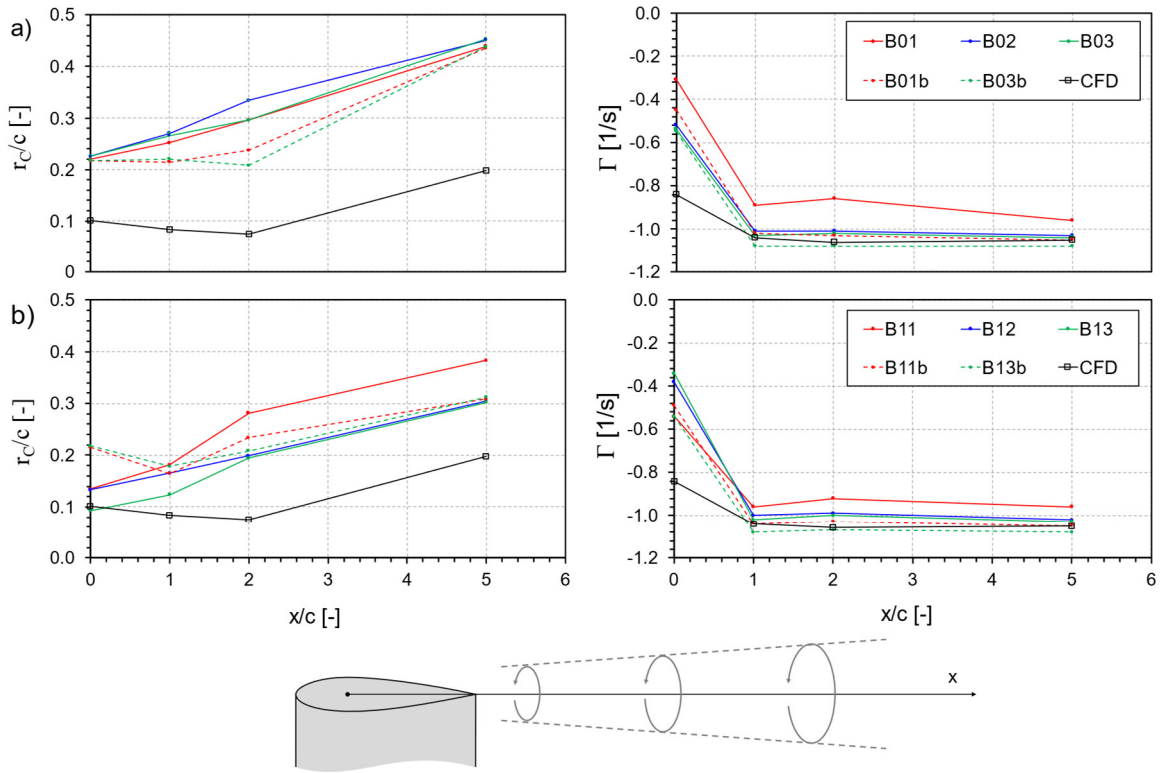

Figure 5. Comparison between baseline ALM and CFD in terms of tip vortex structure: (a) β/c=0.2 (b) β/c=0.1

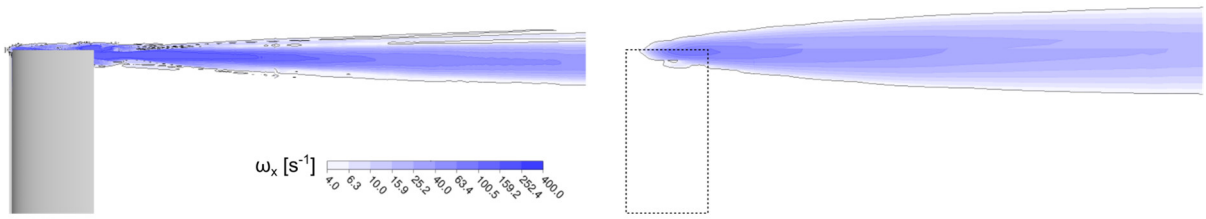

Figure 6. Comparison between baseline CFD (left) and ALM (right) and in terms of streamwise vorticity ω_x

The vortex core radius r_C and its decay are instead directly related to the kernel width β/c. Smaller kernel dimensions in particular correspond to a tighter core and a slower decay rate as the vortex develops downstream (aging). As shown in Figure 5, a proper tuning of this value to β/c=0.1c enables the ALM to provide a satisfying estimation of the CFD vortex characteristics, especially in the near wake (x/c <=1). The vortex aging speed in the far wake is nonetheless largely overestimated with respect to CFD (see Figure 6), with a r_C value 50% higher at x/c=5. Such discrepancy, although partially connected by the inevitable difference in grid resolution between ALM and blade-resolved simulations, is in the authors' view probably related to the absence of the physical blade tip in the ALM approach and its effect on vortex dynamics, especially turbulence.

Although the ALM, despite the limitations described so far, can provide a fairly good approximation of the three-dimensional flow field developing around the wing, the behaviour of the predicted blade loads is completely unphysical. From Figure 4 it can be observed how, independently from the adopted numerical set-up, the ALM section lift tends in fact to increase towards the tip, instead of going to zero as in blade-resolved simulations and experiments. The reason for such phenomenon, already observed in previous studies [9,10], will be investigated in a future work.

Based on the previous considerations, the mesh B11b (β/c=0.1, N=30, bias factor f=1.08) was selected for the following fixed-wing and rotor simulations, as the most accurate and efficient one.

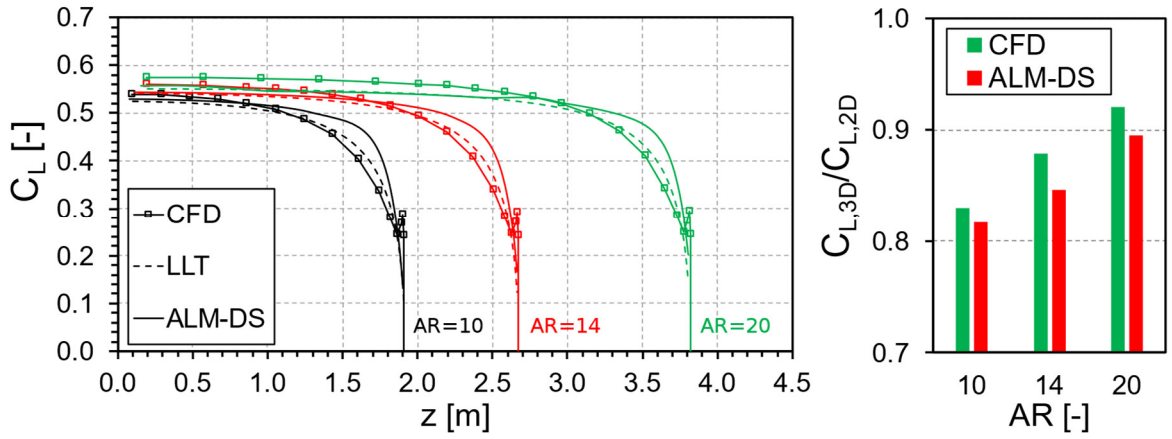

Figure 7. Comparison between corrected ALM, LLT and CFD for different Aspect Ratios (AR)

The application of the Dağ-Sørensen correction notably improves the description of the load profile along the span with respect to the baseline method. This is particularly evident in Figure 7, where the results of corrected ALM simulations are compared against LLT and blade-resolved CFD data for three different Aspect Ratios (AR) and α=6°. The ALM nonetheless still tends to overestimate the section lift coefficient in the last 20% of the blade with respect to the other datasets, i.e., underestimate the vortex induced downwash. This might be related to the DG model own formulation or to its coupling to the proposed ALM tool, in particular with the *LineAverage* velocity sampling technique.

3.3. Rotor simulations

Figure 8 shows the comparison in terms of blade spanwise torque coefficient C_M, normalised over the midspan value, between the ALM with the Glauert and DS correction and the benchmark blade-resolved CFD data over one rotor revolution. In contrast with the Glauert model, which for some angular position yields unphysical results, the DS one allows one to obtain fair agreement with the reference data both in low- and high-load conditions. As already observed for the fixed-wing simulations nonetheless (see Section 3.1), this formulation tends to overestimate blade loading in the last 20% of the blade, especially at the higher angle of attacks ($45° < \theta < 90°$).

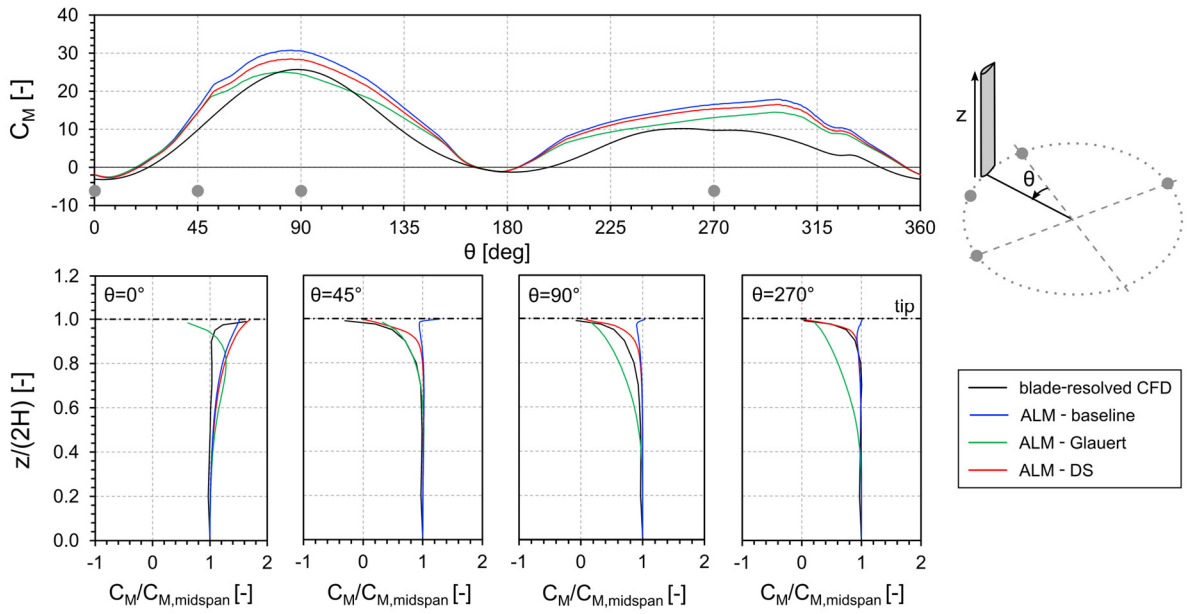

Figure 8. Comparison between ALM and CFD for the one-blade rotor

4. Conclusions

The study presents a comprehensive investigation on the Actuator Line capability to simulate the impact of tip effects on the behaviour of both fixed and rotating blades. The baseline formulation, although capable of predicting the tip vortex structure with a sufficient level of approximation, fails in reconstructing the blade load degradation towards the tip. This major flaw of the ALM approach is solved via the novel hybrid ALM-LLT model proposed by Dağ and Sørensen, here adapted to VAWT simulation. The achieved accuracy gain is noteworthy, especially when compared to the current approaches such as the Glauert correction. Nonetheless, some issues are still present in the last 20% of the blade, where the DS correction tends to overestimate the section loads. This is a known issue of the method that is still under investigation also for horizontal-axis wind turbines and future work will be directed at trying to address it.

References

[1] Ferreira C S, Van Bussel G and Van Kuik G 2007 2D CFD simulation of dynamic stall on a vertical axis wind turbine: Verification and validation with PIV measurements Collection of Technical Papers - 45th AIAA Aerospace Sciences Meeting vol 23 pp 16191–201
[2] Sørensen J N and Shen W Z 2002 Numerical Modeling of Wind Turbine Wakes *J. Fluids Eng* **124** 393–9
[3] Balduzzi F, Marten D, Bianchini A, Drofelnik J, Ferrari L, Campobasso M S, Pechlivanoglou G, Nayeri C N, Ferrara G and Paschereit C O 2018 Three-dimensional aerodynamic analysis of a

darrieus wind turbine blade using computational fluid dynamics and lifting line theory *Journal of Engineering for Gas Turbines and Power* **140**
[4] Shives M and Crawford C 2013 Mesh and load distribution requirements for actuator line CFD simulations *Wind Energy* **16** 1183–96
[5] Martínez-Tossas L A, Churchfield M J and Meneveau C 2016 A Highly Resolved Large-Eddy Simulation of a Wind Turbine using an Actuator Line Model with Optimal Body Force Projection *J. Phys.: Conf. Ser.* **753** 082014
[6] Jha P K, Churchfield M J, Moriarty P J and Schmitz S 2014 Guidelines for Volume Force Distributions Within Actuator Line Modeling of Wind Turbines on Large-Eddy Simulation-Type Grids *J. Sol. Energy Eng* **136** 031003
[7] Churchfield M J, Schreck S J, Martinez L A, Meneveau C and Spalart P R 2017 An Advanced Actuator Line Method for Wind Energy Applications and Beyond *35th Wind Energy Symposium* (American Institute of Aeronautics and Astronautics)
[8] Martínez-Tossas L A and Meneveau C 2019 Filtered lifting line theory and application to the actuator line model *Journal of Fluid Mechanics* **863** 269–92
[9] Dağ K O and Sørensen J 2020 A new tip correction for actuator line computations *Wind Energy* **23** 148–60
[10] Meyer Forsting A R, Pirrung G R and Ramos-García N 2019 A vortex-based tip/smearing correction for the actuator line *Wind Energy Science* **4** 369–83
[11] Melani P F, Balduzzi F, Ferrara G and Bianchini A 2021 Tailoring the actuator line theory to the simulation of Vertical-Axis Wind Turbines *Energy Conversion and Management* **243** 114422
[12] Balduzzi F, Drofelnik J, Bianchini A, Ferrara G, Ferrari L and Campobasso M S 2017 Darrieus wind turbine blade unsteady aerodynamics: a three-dimensional Navier-Stokes CFD assessment *Energy* **128** 550–63
[13] Glauert H 1935 Airplane Propellers ed W F Durand (Berlin, Heidelberg: Springer) pp 169–360
[14] Melani P F, Balduzzi F, Ferrara G and Bianchini A 2020 How to extract the angle attack on airfoils in cycloidal motion from a flow field solved with computational fluid dynamics? Development and verification of a robust computational procedure *Energy Conversion and Management* **223** 113284
[15] Balduzzi F, Holst D, Melani P F, Wegner F, Nayeri C N, Ferrara G, Paschereit C O and Bianchini A 2021 Combined Numerical and Experimental Study on the Use of Gurney Flaps for the Performance Enhancement of NACA0021 Airfoil in Static and Dynamic Conditions *Journal of Engineering for Gas Turbines and Power* **143**
[16] Dossena V, Persico G, Paradiso B, Battisti L, Dell'Anna S, Brighenti A and Benini E 2015 An Experimental Study of the Aerodynamics and Performance of a Vertical Axis Wind Turbine in a Confined and Unconfined Environment *J. Energy Resour. Technol* **137** 051207
[17] Drela M 1989 XFOIL: An Analysis and Design System for Low Reynolds Number Airfoils *Conference on Low Reynolds Number Airfoil Aerodynamics* (University of Notre Dame)
[18] Bianchini A, Balduzzi F, Rainbird J, Peiro J, Graham J M R, Ferrara G and Ferrari L 2015 An Experimental and Numerical Assessment of Airfoil Polars for Use in Darrieus Wind Turbines. Part 1 - Flow Curvature Effects *Journal of Engineering for Gas Turbines and Power* **138** 032602-032602–10
[19] Shen W Z, Zhu W J and Sørensen J N 2014 Study of tip loss corrections using CFD rotor computations *J. Phys.: Conf. Ser.* **555** 012094
[20] Anderson J D, Corda S and Van Wie D M 1980 Numerical lifting line theory applied to drooped leading-edge wings below and above stall *Journal of Aircraft* **17** 898–904
[21] Jeong J and Hussain F 1995 On the identification of a vortex *Journal of Fluid Mechanics* **285** 69–94
[22] Mauz M, Rautenberg A, Platis A, Cormier M and Bange J 2019 First identification and quantification of detached-tip vortices behind a wind energy converter using fixed-wing unmanned aircraft system *Wind Energy Science* **4** 451–63